Editors' Suggestion

Synthesis of Quantum Antennas for Shaping Field Correlations

A. Mikhalychev,[1] D. Mogilevtsev,[1,*] G. Ya. Slepyan,[2] I. Karuseichyk,[1] G. Buchs,[3] D. L. Boiko,[3] and A. Boag[2]

[1]*Institute of Physics, Belarus National Academy of Sciences, Nezavisimosti Avenue 68, Minsk 220072, Belarus*

[2]*School of Electrical Engineering, Tel Aviv University, Tel Aviv 69978, Israel*

[3]*Centre Suisse d'Electronique et de Microtechnique (CSEM), Jaquet-Droz 1, 2002 Neuchâtel, Switzerland*

(Received 25 September 2017; revised manuscript received 9 October 2017; published 22 February 2018; corrected 6 April 2018)

We present a method to design an initial state in a quantum antenna in order to shape the emitted field higher-order correlation functions at will. This method is based on quantum state reconstruction techniques and relies on an entanglement of the emitters. We show that even the simplest antenna arrangements such as linear dipole arrays can exhibit a large variability in the emitted field-correlation function patterns, including, e.g., the generation of highly codirectional and contradirectional correlated twin photons, as well as multiphoton entangled states. Moreover, we identify a class of initial states that lead to a complete suppression of the field in the far-field zone. We also demonstrate the possibility to use a modified semiclassical approach for designing quantum antennas, simplifying the antenna state inference task. Our approach can find applications in the development of future quantum optics devices and methods, such as quantum sources for superresolution quantum imaging, high-precision sensing, as well as emitter-field interfaces for quantum information processing systems.

DOI: 10.1103/PhysRevApplied.9.024021

I. INTRODUCTION

Classical antennas are devices transforming radio waves from free space to a guiding device and vice versa [1]. The radiative properties of such antennas are characterized by the angular distribution of the radiated field and intensity (field- and power-radiation patterns). In the case of classical radiation, the power-radiation pattern formed by interference effects is equal to the squared modulus of the field-radiation pattern divided by the doubled characteristic impedance of the medium [1]. However, this simple picture does not hold for nonclassical states of emitted radiation. For example, the field-radiation pattern can vanish, whereas the power-radiation pattern has a finite nonzero value. Generally, higher-order correlation functions of the nonclassical field cannot be expressed through lower-order ones.

Recent progress in nanofabrication opened a way for the design and implementation of nanoantennas operating in the terahertz, infrared, and visible spectral ranges [2–5]. In spite of the quantum origin of charge-carrier transport inside the antennas, the emitted field was commonly considered as being classical. However, the use of the quantum properties of light and generalization of the concept of antennas for the quantum case [6–10] open far richer possibilities for controlling and shaping the emitted field (e.g., directive light squeezing via antenna emission [10]). Note that light squeezing can be achieved not only by arranging emitters, but also by engineering the initial state of the antenna. It is well known that an entangled state of emitters can lead to entanglement of the emitted photons (i.e., the state of the field can be mapped into the emitters state and vice versa). This effect was suggested as a basis for a quantum memory device capable of storing entangled states of light [11,12]. Furthermore, entanglement of emitters in antennas can lead to intensity distributions otherwise impossible to reach with the factorized initial states of the antenna emitters [13], to sub-Rayleigh imaging and superresolution [14,15], as well as to superbunching [16]. Until now, quantum features in the field emitted by an antenna were mostly considered for some well-known initial states independently of the actual antenna geometry (e.g., symmetric Dicke states were usually considered [13]). On the other hand, so-called "timed" Dicke states bear information about the location of emitters [17] and provide a special quantum mechanism that introduces a nonreciprocity of the antenna [6].

Here, we introduce a method to design an initial state in a quantum antenna in order to shape the emitted field-correlation functions. The nonclassicality of the antenna's radiation is revealed through a measurement of the higher-order correlation functions. Note that such a measurement constitutes a convenient imaging tool [18] that enables us to reach superresolution [19–21]. The approach introduced here is similar to the one usually implemented in quantum-state tomography. In the same spirit, one can optimize the

*Corresponding author.
d.mogilevtsev@ifanbel.bas-net.by

directivity of the correlation functions of the radiation produced by a quantum antenna. For example, by optimizing the second-order correlation function of the two-particle entangled state of an equispaced linear antenna array, we can produce photon pairs that are strongly correlated in momentum. Interestingly, we find that both codirectional and contradirectional correlations are possible for the same spatial antenna design, but with different initial states. The same approach is also valid for multiparticle antenna states and higher-order correlation functions. In particular, we show that some initial states lead to a strong suppression of the radiation in the far-field zone, reproducing a classical effect of "nonradiative source" [1,22]. Additionally, we show that in some cases, the quantum correlations of the antenna field can be captured with a semiclassical model of the emitter-field interaction.

The outline of the paper is as follows. In the Sec. II, the antenna model is introduced. In Sec. III, we describe the procedure for designing the antenna state with the required correlation functions. In the Sec. IV, the long-time field state is considered for providing guidelines for the field shaping. Section V discusses the example of co- and contradirectional twin-photon propagation, and Sec. VI considers a suppression of the far-field radiation. Finally, Sec. VII discusses an application of a semiclassical approach in the description of the field emitted by a quantum antenna.

II. ANTENNA MODEL

As a model system for a quantum antenna, we consider a chain of N identical noninteracting two-level emitters with the same dipole moments $\vec{d}$ positioned along the same axis at points $\vec{R}_j$ (see Fig. 1). Omitting the time-dependence factor, which is common for all emitters, the positive-frequency field operator part that gives nonzero contribution to the normally ordered correlation functions and describes the spatial field distribution at the point $\vec{r}$ in the far-field zone, reads

$$\vec{E}(\vec{r}) \propto A(\vec{r}) = \sum_{j=1}^{N} \frac{\vec{n}\times[\vec{n}\times\vec{d}]}{|\vec{r}|} \exp\{i\omega(|\vec{R}_j - \vec{r}|/c)\}\sigma_j^-, \qquad (1)$$

where $\sigma_j^- = |-_j\rangle\langle+_j|$ is the lowering operator for the jth two-level system (TLS) with upper (lower) levels described by the vectors $|\pm_j\rangle$, and $\vec{n}$ being the unit vector from an emitter to the observation point; ω being the TLS transition frequency. For what follows, we label the right-hand side in Eq. (1) as the array factor operator $A(\vec{r})$. Generically, the design of an antenna consists in finding the positions $\vec{R}_j$ of individual TLS elements, and in defining the initial density matrix of the antenna ρ in a way to achieve the required values of the simultaneous correlation function of the order n in some sets $\{l\}$ of directions $\{\vec{r}_{k,l}\}$, $k = 1, \ldots, n$:

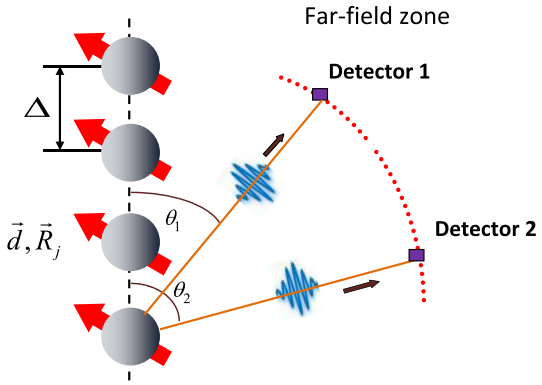

FIG. 1. Schematics of an equispaced linear array antenna. The second-order correlations can be detected by measuring simultaneous counts at detectors D_1 and D_2. The red arrows represent the TLS dipole moments of the antenna. The dipole moments of every TLS are the same.

$$G^{(n)}(\vec{r}_{1,l}, \ldots, \vec{r}_{n,l}) = \left\langle \left[\prod_{k=1}^{n} A(\vec{r}_{k,l})\right]^{\dagger} \prod_{k=1}^{n} A(\vec{r}_{k,l}) \right\rangle. \qquad (2)$$

Thus, the index l in Eq. (2) labels different spatial arrangements of the n detectors. These functions can be directly measured by placing photon detectors in given directions and by recording the coincident counts (for example, the scheme for measuring $G^{(2)}$ is depicted in Fig. 1). Note that for a conventional classical antenna, the radiation pattern and all correlation functions are entirely defined by the average field amplitude $\langle E(\vec{r})\rangle$. However, in the quantum case the situation is different. For example, for all TLSs being either in the excited or ground state, $\langle E(\vec{r})\rangle = 0$ for an arbitrary $\vec{r}$, whereas one can have $G^{(n)} \neq 0$.

III. STATE ESTIMATION FOR ANTENNAS

The problem of antenna state design can be formulated as a state estimation problem in the following way. We specify a finite number of discrete sets of spatial observation points for which we will perform the antenna design $\{\vec{r}_{k,l}\}$, and rewrite Eq. (2) as

$$p_l = \mathrm{Tr}\{\Pi_l \rho\}, \Pi_l \propto \left[\prod_{k=1}^{n} A(\vec{r}_{k,l})\right]^{\dagger} \prod_{k=1}^{n} A(\vec{r}_{k,l}), \qquad (3)$$

where the operators Π_l are semipositive definite and can be considered as elements of a positive operator valued measure, while p_l can be considered as the set of targeted probabilities. Generally, Π_l can be singular and might not form a complete set required for an unambiguous representation of the antenna state. The visibility operator that comprises all possible arrangements of the detectors is $C_V = \sum_{\forall\, l} \Pi_l$ [23]. This operator defines the subspace of states accessible for measurements [and normalization of the set of probabilities (3)]. The operator C_V can be singular

too and different from the unity operator. Thus, an exact solution for the density matrix might not exist for some subsets of targeted probabilities. Therefore, here we consider the problem of shaping the correlation function in the following way: we look for the density matrix (estimator) maximizing the probabilities p_s of some subset $\{s\}$, while simultaneously minimizing other probabilities p_m, $m \in \{l\}\backslash\{s\}$. Assuming that

$$0 \le p_l^{\text{low}} \le p_l \le p_l^{\text{high}}, \tag{4}$$

$p_l^{\text{low(high)}}$ being the lower (upper) limit of the targeted probabilities, our design problem can be formulated as a minimization of some distance between target and estimated sets, $D(p_{\text{target}}, p_l)$, where the set of the targeted values is $\{p_m^{\text{low}}, p_s^{\text{high}}\}$. Like the directivity problem for a classical antenna [1], the problem of maximizing the directivity of the quantum antenna can be formulated in the following way: we look for a conditional minimum of $\text{Tr}\{C_V\rho\}$ under the conditions (4) and for $\rho \ge 0$. Note that defining an available target range is a semidefinite programming problem of finding $\min(\max)\{p_l\}$ for $\rho \ge 0$. As an example, let us take an antenna in the pure two-excitation state: $\rho = |\psi\rangle\langle\psi|$, where

$$|\psi\rangle = \sum_{j=2}^{N}\sum_{m=1}^{j-1} c_{jm}|+_j, +_m\rangle, \tag{5}$$

with the summation performed over all distinct pairs of indices $(j, m) \in [1, N]$. The vectors $|+_j, +_m\rangle$ describe the state of excited jth and mth TLSs with all other TLSs in the lower state. The state (5) can be generated in a number of ways, for example, by controlling the interaction between dipoles [24], for example, for atoms in Rydberg states [25] or for trapped ions [26], or using the method applied for quantum memory, when the desired state can be created by the combination of driving fields in appropriately chosen states [27,28]. Such emitter-field interfacing is researched and applied for a wide range of materials, including laser-cooled gases and trapped atoms, impurity-doped crystals, semiconductors, and even optomechanical systems.

An example of available targeted regions for the state (5) in array with $N = 20$ is shown in Fig. 2. This example is calculated by optimization over all the coefficients c_{jm} in Eq. (5) for just one pair of $G^{(2)}(\theta_1, \theta_2)$ directions, $\cos\theta_1 = 0$, $\cos\theta_2 = 0.05$. The available range of $p(\theta_2, \theta_2)$ (solid line) and $p(\theta_1, \theta_2)$ (dotted line) is found under the condition that $p(\theta_1, \theta_1)$ has some fixed value. One can see that limitations on possible choices of targeted probabilities can be quite severe.

IV. FIELD-STATE CONSIDERATIONS

To give an intuitive picture of the connection between the state of the antenna and the field-correlation functions, let us consider the field of the antenna in the momentum space. Initially, let us assume that the antenna initial state is a product of the states of the first M fully excited emitters and N-M emitters in the ground state. For time intervals much longer than the inverse decay rate of the excited state γ, the field disentangles from the emitters and can be written as [29]

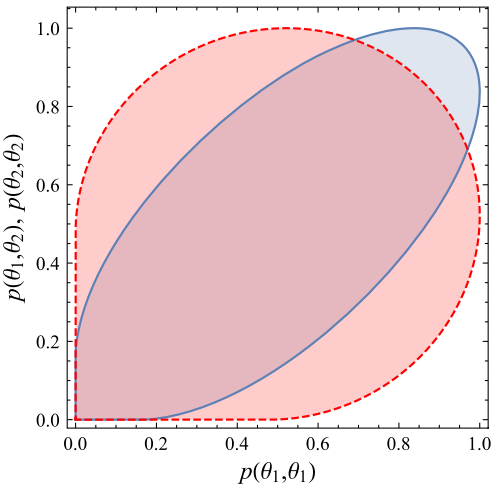

FIG. 2. An example of accessible regions of target probabilities for shaping $G^{(2)}$ by a set of $N = 20$ equidistant TLS antennas depicted in Fig. 1 for the angles $\cos\theta_1 = 0$, $\cos\theta_2 = 0.05$ and two-excitation pure states of the form given in Eq. (5). The dashed curve delimits the region of available probabilities $p(\theta_1, \theta_2)$ versus $p(\theta_1, \theta_1)$; the solid line delimits the region of available $p(\theta_2, \theta_2)$ versus $p(\theta_1, \theta_1)$. Each probability $p(\theta_j, \theta_k)$, j, $k = 1, 2$ is normalized by its maximal possible value.

$$|\Psi\rangle \propto \int \prod_{j=1}^{M} [d^3\vec{k}_j a_j^\dagger(\vec{k}_j) V(\vec{k}_j)] \Phi(\{\vec{k}_j\}, \{\vec{R}_j\})|\text{vac}\rangle, \tag{6}$$

where the function

$$V(\vec{k}_j) = \frac{\sqrt{w(\overrightarrow{k_j})}\vec{d}\,\vec{e}(\overrightarrow{k_j})}{w(\vec{k}_j) - \omega + i\gamma/2}$$

does not depend on the positions of the emitters. The function

$$\Phi(\{\vec{k}_j\}, \{\vec{R}_j\}) = \exp\left\{-i\sum_{j=1}^{M}\vec{k}_j\vec{R}_j\right\} \tag{7}$$

describes the relative phase shifts introduced by the locations of the TLSs and the detectors. Here, $a_j^\dagger$ is the creation operator for the mode with momentum $\vec{k}_j$, frequency $w(\vec{k}_j)$, and polarization vector $\vec{e}(\vec{k}_j)$; $|\text{vac}\rangle$ is the vector of the field vacuum; and ω is the TLS transition frequency. Equations (6) and (7) give a hint for understanding the

mechanism of $G^{(2)}$ shaping. Let us take again, for example, the simple two-excitation pure state (5) with $c_{jm} = \delta_{m,N+1-j}/\sqrt{N}$. For such an initial state of the antenna, the wave function of the emitted field state is of the form (6) with

$$\begin{aligned}\Phi(\{\vec{k}_j\},\{\vec{R}_j\}) &= \frac{1}{\sqrt{N}}\sum_{m=1}^{N}\exp\{-im(\vec{k}_1+\vec{k}_2)\vec{\Delta}\}\\ &\quad\times\exp\{-i(\vec{k}_1+\vec{k}_2)\vec{R}_0 - i\vec{k}_1\vec{\Delta}(N+1)/2\},\\ &= \exp\{-i(\vec{k}_1+\vec{k}_2)\vec{R}_0\}\\ &\quad\times\frac{\sin\{N(\vec{k}_1-\vec{k}_2)\vec{\Delta}/2\}}{\sqrt{N}\sin\{(\vec{k}_1-\vec{k}_2)\vec{\Delta}/2\}},\end{aligned} \tag{8}$$

where the vector $\vec{\Delta} = \vec{R}_{m+1} - \vec{R}_m$ does not depend on m, and $\vec{R}_0$ is the vector describing the position of the antenna middle point. The function $|\Phi|$ in Eq. (8) for $N \gg 1$ has a sharp peak at $(\vec{k}_1 - \vec{k}_2)\vec{\Delta} = 0$ and tends towards the delta function $\delta((\vec{k}_1 - \vec{k}_2)\vec{\Delta})$ when $N \to \infty$. This function is not factorable with respect to momenta $\vec{k}_j$, thus, the state (6) is entangled in momentum. Hence, one should expect a sharp maximum in the second-order correlation function $G^{(2)}$, corresponding to codirectionally emitted photons.

Similarly, Eq. (7) points to the possibility of emitting multiphotons momentum-entangled states and to shape higher-order correlation functions even using the simplest linear array antenna of Fig. 1. Indeed, a superposition of at least two different sets of initially excited antenna TLSs leads to a nonfactorability of the function $\Phi(\{\vec{k}_j\},\{\vec{R}_j\})$ and thus to momentum entanglement of the wave function (6). Let us demonstrate this effect on the example of a three-photon state with the initial antenna state $|\psi\rangle = (1/\sqrt{N-2})\sum_{j=1}^{N-2}|+_j,+_{j+1},+_{j+2}\rangle$. We obtain

$$\begin{aligned}\Phi_l(\{\vec{k}_j\},\{\vec{R}_j\}) &= 2\exp\{-i(\vec{k}_1+\vec{k}_2+\vec{k}_3)\vec{R}_0\}\\ &\quad\times\frac{\sin\{(N-2)(\vec{k}_1+\vec{k}_2+\vec{k}_3)\vec{\Delta}/2\}}{\sqrt{N-2}\sin\{(\vec{k}_1+\vec{k}_2+\vec{k}_3)\vec{\Delta}/2\}}\\ &\quad\times\left(\cos\left\{\frac{(\vec{k}_1-\vec{k}_2)\vec{\Delta}}{2}\right\}+\cos\left\{\frac{(\vec{k}_1-\vec{k}_3)\vec{\Delta}}{2}\right\}\right.\\ &\quad\left.+\cos\left\{\frac{(\vec{k}_2-\vec{k}_3)\vec{\Delta}}{2}\right\}\right),\end{aligned} \tag{9}$$

with $|\Phi|$ being not factorable and approaching the delta function $\delta((\vec{k}_1+\vec{k}_2+\vec{k}_3)\vec{\Delta})$ for $N \to \infty$. The correlation function $G^{(3)}$ is sharply peaked for angles satisfying the condition $(\vec{k}_1+\vec{k}_2+\vec{k}_3)\vec{\Delta} = 0$.

V. QUANTUM ANTENNA SYNTHESIS FOR DIRECTIONAL TWO-PHOTON EMISSION

To demonstrate the feasibility of our antenna design approach, we apply it to the simple case of twin-photon generation by the linear antenna in Fig. 1 with initial states (5). We aim to find the coefficients c_{jm} that provide a desired spatial pattern of the second-order correlation function $G^{(2)}$. Taking into account considerations from the previous section, we consider the optimization of $G^{(2)}$ for twin-photon emission from a finite length linear array antenna.

A. Codirectional two-photon emission

From Eqs. (1) and (2) the second-order correlation function in the plane perpendicular to the orientation of the dipoles is given by

$$\begin{aligned}G^{(2)}(\theta_1,\theta_2) &\propto p(\theta_1,\theta_2) = \mathrm{Tr}\{\Pi(\theta_1,\theta_2)\rho\},\\ \Pi(\theta_1,\theta_2) &= \sum_{j,m,n,q}\exp\{ik\Delta(j-n)\cos(\theta_1)\}\\ &\quad\times\exp\{ik\Delta(m-q)\cos(\theta_2)\}\sigma_j^+\sigma_m^+\sigma_n^-\sigma_q^-,\end{aligned} \tag{10}$$

where k is the wave number and Δ is the distance between the dipoles; $\theta_{1,2}$ are the angles in the direction of the detectors. Optimization of the antenna directivity for this case can be formulated as a quadratic programming problem of minimizing the average visibility operator $\langle\psi|C_V|\psi\rangle$ subjected to conditions (4). Let us aim, for example, to obtain the codirectional correlation of emitted photons, i.e., a sharply peaked $G^{(2)}$ pattern for $\theta_1 = \theta_2$. Figures 3(a) and 3(b) show the results of such optimization for $k\Delta = 2$. The optimization is done by minimizing the weighted sum of the average visibility operator $\langle\psi|C_V|\psi\rangle$ and the quadratic distance between the actual values of $p(\theta_i,\theta_i;c_{jm})$ as well as the targeted value p_0 for 100 discrete angles θ_i in the range $[0,\pi]$. For the TLS number N varying from 2 to 10, the problem is solved for the general case of complex coefficients $c_{jm} \in \mathbb{C}$. However, the imaginary parts of the optimal solution turn out to be very small in comparison with the real parts of c_{jm}. Therefore, for antennas with a larger number of TLSs (we checked up to $N = 20$), these coefficients are assumed to be real: $c_{jm} \in \mathbb{R}$. Indeed, in Fig. 3(a) one can see that $G^{(2)}$ is sharply peaked around equal observation angles. The initial antenna state producing such correlations is shown in Fig. 3(b). Remarkably, in accordance with the field-state considerations of the previous section, we obtain that $c_{j,N+1-j} \approx 1/\sqrt{N}$, while all other coefficients are much smaller. The initial state corresponds to excited pairs of the dipoles located symmetrically on the opposite sides of the antenna [e.g., the first and the last one, the second and the $(N-1)$th, etc.]. Figures 3(c) and 3(d) show the

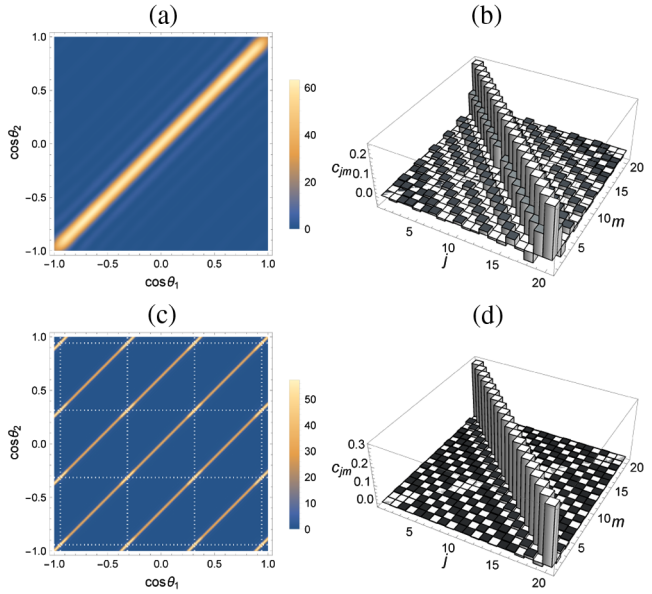

FIG. 3. (a),(c) The normalized $G^{(2)}(\theta_1,\theta_2)$ [i.e., $p(\theta_1,\theta_2)$ of Eq. (10)] obtained as the result of optimization for the generation of two codirectional photons; (b),(d) states in Eq. (5) obtained as the result of optimization. For all panels, $N = 20$; for panels (a), (b) $k\Delta = 2$, for panels (c),(d) $k\Delta = 10$. Dashed lines divide the plot in panel (c) into equivalent regions due to the periodicity of the signal for $k\Delta > \pi$.

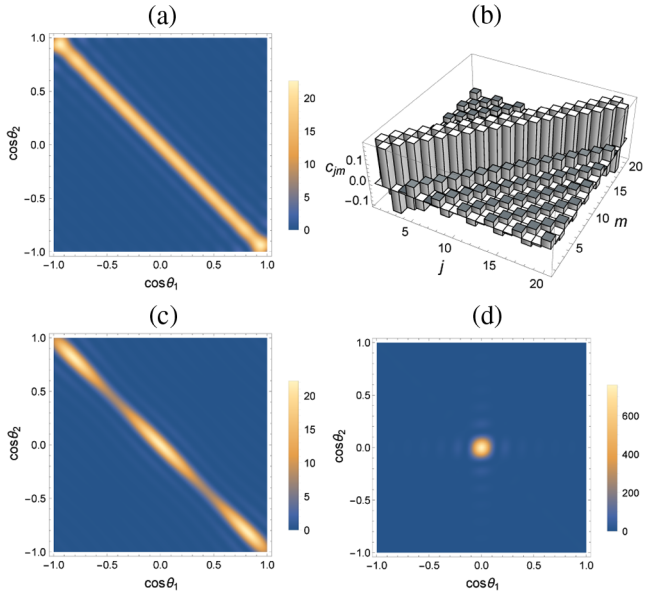

FIG. 4. (a),(c) The normalized $G^{(2)}(\theta_1,\theta_2)$ obtained as the result of numerical and analytical optimization for the generation of two contradirectional photons, respectively. (b) The state in Eq. (5) obtained as the result of numerical directivity optimization. (d) The normalized $G^{(2)}(\theta_1,\theta_2)$ obtained as the result of optimization for the generation of two photons emitted in a direction perpendicular to the antenna. For all panels, $N = 20$; $k\Delta = 2$.

optimization results for the larger distance between dipoles, i.e., $k\Delta = 10$. The radiation pattern is still sharply peaked around $\theta_1 = \theta_2$, but in contrast to the previous example, each emission direction of one photon is correlated to several possible emission directions of the second photon. To elucidate the origin of this pattern, we rewrite Eq. (10) as

$$p(\theta_1,\theta_2) = \langle\psi|\Pi(\theta_1,\theta_2)|\psi\rangle = |\Phi(\theta_1,\theta_2)|^2 \equiv \left|\sum_{j,m=1}^{N} c_{jm}\exp\{-ik\Delta(j\cos\theta_1 + m\cos\theta_2)\}\right|^2. \tag{11}$$

Indeed, it can be seen that $\Phi(\theta_1,\theta_2)$ is a periodic function of $\cos\theta_1$ and $\cos\theta_2$, that is, $\Phi(\theta_1,\theta_2) = \Phi(\theta_1,\theta_2')$ if $k\Delta(\cos\theta_2 - \cos\theta_2') = 2\pi n$ with integer n.

B. Contradirectional two-photon emission

By tailoring the initial quantum antenna state, one can also achieve contradirectional correlations between emitted photons. The optimization results for the radiation pattern with $G^{(2)}$ sharply peaked around $\theta_2 = \pi - \theta_1$ are shown in Fig. 4(a), which attests to strong contradirectional correlations. The optimal initial state of the antenna [Fig. 4(b)] shows a peculiar structure of the matrix c_{jl} describing the state (5). This matrix is composed of sets of the coefficients with equal amplitudes on each subdiagonal, i.e., coefficients $c_{j,j\pm l} = c_l$ do not depend on the index j. Once again, this feature can also be explained using field-state considerations on the basis of Eqs. (6) and (7) in the following way. Let us consider the contribution from just one subdiagonal of the matrix $c_{j,j+l}$ with index shift l (i.e., we assume $c_l = 1/\sqrt{N-l}$ and $c_{l'} = 0$ for all other subdiagonals with $l' \neq l$). The wave function of the emitted field state is described by Eq. (6) with

$$\Phi_l(\{\vec{k}_j\},\{\vec{R}_j\}) = 2\exp\{-i(\vec{k}_1+\vec{k}_2)\vec{R}_0\} \times\cos\left\{\frac{l}{2}(\vec{k}_1-\vec{k}_2)\vec{\Delta}\right\} \times\frac{\sin\{(N-l)(\vec{k}_1+\vec{k}_2)\vec{\Delta}/2\}}{\sqrt{N-l}\sin\{(\vec{k}_1+\vec{k}_2)\vec{\Delta}/2\}}. \tag{12}$$

For $N\to\infty$ and finite l the function $|\Phi_l|$ asymptotically tends toward the delta function $\delta((\vec{k}_1+\vec{k}_2)\vec{\Delta})$, which corresponds to an entangled two-photon state with strong contradirectional correlations. However, in contrast to the previous example in Sec. V A, the absolute value of the wave function is varied along the line $\vec{k}_2\vec{\Delta} = -\vec{k}_1\vec{\Delta}$ ($\theta_2 = \pi - \theta_1$) as $\cos(lk\Delta\cos\theta_1)$. In order to obtain a $G^{(2)}$ pattern with even contradirectional correlations as shown in Fig. 4(a), one needs to combine several subdiagonal sets $c_{j,j\pm l} = c_l$ with different subdiagonal

numbers l. Figure 4(c) shows the result of such a combination for three sets with $l = 1, 2, 3$ and relative amplitudes $c_1 : c_2 : c_3 = 1 : -0.7 : 0.4$. The state shows strong contradirectional correlations across the full range of angles [see the main diagonal in the pattern of Fig. 4(c)], but still it gives a less even and less sharply directed pattern of $G^{(2)}$ than the state found by numerical optimization in Fig. 4(b).

C. Maximal directivity of emission

As a particular example, one can consider a state with the maximal directivity of two-photon emission in the direction perpendicular to the linear array antenna ($\theta_1 = \theta_2 = \pi/2$). The radiation pattern for the numerically optimized state is shown in Fig. 4(d). As one would expect, the optimal state is close to the symmetric two-excitation Dicke state with $c_{jm} = \text{const}$ for all indexes j and m.

VI. "DARK" STATES AND ANTENNA DESIGN

A. Finding the dark state

Localization of the emitted field inside a finite volume is something that one would really expect for such exquisitely designed objects as 3D photonic crystals and metamaterial structures [30,31]. With classical antennas, one can specifically design such distributions of currents so as to obtain the same effect, that is, to create a nonradiative source [1,22]. Counterintuitively, this effect can also be achieved in a simple regular linear antenna array by choosing the appropriate initial quantum state of the antenna. Just by minimizing $G^{(2)}(\theta_1, \theta_2)$ for all angles θ_1 and θ_2, one obtains the initial state of the antenna leading to a strong field suppression in the far-field zone. Indeed, let us minimize the average visibility operator $\langle\psi|C_V|\psi\rangle$ for the state (5) without imposing any additional requirements to obtain bright spots or lines in the $G^{(2)}$ patterns. For $k\Delta < \pi$, such optimization can be successfully performed [Fig. 5(a)], yielding the maximum $G^{(2)}$ value in Eq. (10) of 3×10^{-7} for $N = 20$ and $k\Delta = 2$. Equation (12) gives a hint on how to design such a state: first, choose broad distributions of the matrix coefficients describing the state (5) along each subdiagonal, i.e., take $c_{j,j\pm l} \propto f(j-(N+1)/2)$ along subdiagonals to suppress emission outside the region with $\theta_2 \approx \pi - \theta_1$. For example, a Gaussian distribution of the matrix coefficients $f(m) = e^{-m^2/\sigma^2}$ leads to $k\Delta|\cos\theta_1 + \cos\theta_2| \lesssim 2/\sigma$. Then, one should suppress the emission along the diagonal using an appropriate combination of $\cos\{lk\Delta(\cos\theta_1 - \cos\theta_2)/2\}$ [see Eq. (12)]. Here, one can find an approximate analytical expression surprisingly close to the optimal state numerically found in Fig. 5(a), i.e.,

$$c_{jm} \propto (-1)^l l^2 \exp\{-(l^2 + q^2)/(4\sigma^2)\}, \tag{13}$$

where $l = |j - m|$, $q = (j + m) - (N + 1)$, and $\sigma \approx 3.2$. It is worth mentioning that for $k\Delta > \pi$ one cannot design such a dark state. By introducing dimensionless variables $x_j = k\Delta\cos\theta_j$, $j = 1, 2$, $x_j \in [-k\Delta, k\Delta] \supset [-\pi, \pi]$, one can easily see that the following lower bound holds:

$$\int_{-k\Delta}^{k\Delta} dx_1 \int_{-k\Delta}^{k\Delta} dx_2 p(\theta_1, \theta_2) \geq \int_{-\pi}^{\pi} dx_1 \int_{-\pi}^{\pi} dx_2 p(\theta_1, \theta_2) = 2\pi^2 \sum_{j=2}^{N} \sum_{m=1}^{j-1} |c_{jm}|^2 = 2\pi^2, \tag{14}$$

where the function p is defined by Eq. (10) and the normalization of the state (5) is taken into account. Figure 5(b) shows the radiation pattern for $k\Delta = 10$, while the initial state is depicted in Fig. 5(a). One can see in Fig. 5(b) that it is possible to suppress the emission in some regions [blue squares with dashed border in Fig. 5(b)], but not to the whole range of angles. Note that just one square would represent the total radiation pattern for $k\Delta = 2$.

Notice that such quantum nonradiative sources can be useful for enhancing electromagnetic compatibility of nanoelectronic devices, i.e., for suppressing undesirable mutual influence [32].

Remarkably, by unconditionally maximizing the mean value of the visibility operator $\langle\psi|C_V|\psi\rangle$ for the state (5), we can achieve an opposite effect and obtain a nearly homogeneous far-field distribution. An example of such an optimization is shown in Fig. 6. Figure 6(a) shows the

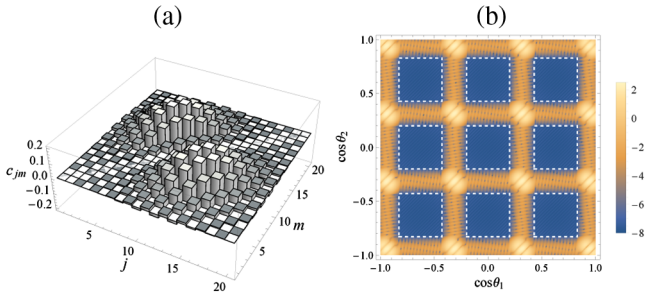

FIG. 5. (a) The "dark" state (5) obtained as the result of the optimization for $N = 20$, $k\Delta = 2$. (b) The pattern of $\log_{10} G^{(2)}(\theta_1, \theta_2)$ for the state (a), calculated for $k\Delta = 10$. Dashed lines define dark regions.

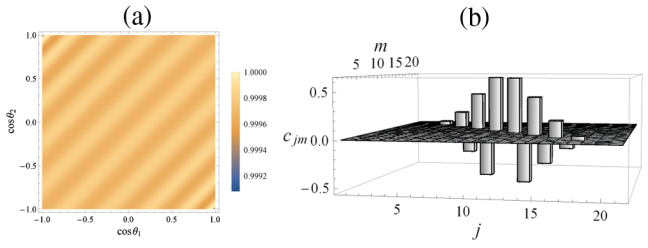

FIG. 6. (a) A nearly homogeneous pattern of $G^{(2)}(\theta_1, \theta_2)$ for the "light" state (b) obtained as the result of the optimization of the state (5) for $N = 20$, $k\Delta = 1$.

radiation pattern for $k\Delta = 1$, while the initial state is depicted in Fig. 6(b).

B. Simultaneous state and antenna design

Interestingly, the field-state considerations also point to the possibility of engineering the initial state and the antenna geometry for a complete 3D suppression of the far field. Indeed, let us take two perpendicular linear antennas with the same dipole moments orthogonal to the antenna plane and randomly located TLSs. We choose the initial state as a superposition of randomly chosen pairs of TLS from the first and second antennas. Then, the phase factor reads

$$\Phi(\{\vec{k}_j\},\{\vec{R}_j\}) \propto \sum_{\forall\, j,m} \exp\{-i(\vec{k}_1\vec{R}_j + \vec{k}_2\vec{R}_m)\}, \qquad (15)$$

where j and m are the indices of the TLSs from the two antenna arms. For a sufficiently large number of TLSs in the antenna, the phase factor in Eq. (15) tends toward zero for all directions $\vec{k}_{1,2}$ except for directions parallel to $\vec{d}$. In this way, the emitted field in the far-field zone is suppressed. However, one should notice that for the states predicting a field localization, the antenna approximation of noninteracting emitters might fail. The localized photons might be reabsorbed and reemitted by the antenna (in Sec. VII below we outline one possible approach to account for such interactions between emitters).

Also, by simultaneously changing the shape and the initial state of the antenna, one can get a high directivity of the correlation function without using the Dicke state as the initial antenna state. Equation (8) hints toward a simple way to obtain co- or contradirectional correlations of emitted photons that are localized in a narrow region in the vicinity of $\pm\pi/2$. More specifically, instead of one regular antenna array shown in Fig. 1(a), let us consider an antenna composed of two regular linear arrays located on the same axis and each comprising N TLSs. We choose the pitch of TLSs in one subantenna to be u times larger than in the other subantenna.

We consider the initial antenna state (5) with excited TLS pairs composed of one counterpart from the first subarray (e.g., with larger pitch) and another counterpart from the second subarray (e.g., with smaller pitch). In this case, the first index of the matrix element c_{jm} enumerates TLS from the subarray with larger pitch while the second index enumerates TLS from the subarray with shorter pitch. As in Sec. V A, we then additionally impose a specific symmetry between indexes of TLS located symmetrically on the opposite sides of antenna arms. More specifically, we define the initial state by nonvanishing coefficients $c_{j,N+1-j} = 1/\sqrt{N}$, where the index j spans over the large-period subarray (the index $N+1-j$ then spans over a short-period subarray). For our compound antenna composed of two subarrays with different pitches, Eqs. (7) and (8) suggest a sharp localization of the emitted photons for $(\vec{k}_1 - \vec{k}_2/u)\vec{\Delta} = 0$, which can be satisfied for $u \gg 1$ only if both $\vec{k}_{1,2}$ are nearly orthogonal to $\vec{\Delta}$.

Thus, we can see that a simultaneous design of the antenna geometry and the initial states opens considerably richer possibilities for the optimization of the correlation functions compared to the state design for a predefined antenna. However, generally, such a design is a complicated nonlinear optimization problem.

VII. SEMICLASSICAL APPROACH

As we have shown, quantum interferences are essential for shaping the correlation functions. Here, we show that it is still possible to use a semiclassical approach for modeling the emitters dynamics and, after a minor modification, to reproduce nonclassical features of the spatial correlation functions $G^{(n)}$ from Eq. (2) (we term this recipe "the postsemiclassical approximation"). Such a recipe can be developed in spite of the fact that the semiclassical approach is, generally, unable to capture the mechanism of spontaneous emission and the effects stemming from it. For example, the creation of entanglement between TLS decaying into the same radiative reservoir [33] can hardly be captured by the approach assuming an absence of quantum correlations between TLSs. Nevertheless, field-correlation effects can still be successfully captured in some cases. The best-known example is superradiance. The onset of cooperative effects and phase correlations leading to the formation of the superradiant field pulse can be quite accurately described by the semiclassical approach [34]. Importantly, the initial state of interacting semiclassical TLS does not need to be correlated. The correlations self-establish at the initial stage of cooperative emission [35].

The key observation enabling us to develop a postsemiclassical approximation is given by Eqs. (1) and (2). They show that by modeling the TLS correlation functions with enough accuracy, one would get an accurate description of the emitted field in the far-field zone. From the first glance, to model correlation functions of noninteracting quantum emitters with correlation functions of interacting semiclassical emitters (notice that interaction is intrinsic for semiclassical models) is hardly possible. However, it is shown that interacting TLS can have spatial correlation functions coinciding with the spatial correlation functions of noninteracting TLS [36]. The task is considerably simplified by requiring closeness of only the spatial correlation patterns for some specific time intervals.

The semiclassical approach in its simplest form assumes a factorization of the correlation functions (2) up to the first-order averages, for example, $\langle\sigma_j^-(t_1)\sigma_k^-(t_2)\rangle \approx \langle\sigma_j^-(t_1)\rangle\langle\sigma_k^-(t_2)\rangle$, where the time dependence of averages $\langle\sigma_j^{\pm}\rangle$ is derived from the semiclassical Maxwell-Bloch equations [34,35] (see also Appendix). First, let us consider semiclassically the antenna with uncorrelated identical

initial states of each TLS. Assuming interacting TLSs, for a sufficiently long antenna ($N \gg 1$) one can, e.g., replace the sum $\sum \Pi_{nq}^{jm}(\theta_1,\theta_2)\langle\sigma_j^+\sigma_m^+\sigma_n^-\sigma_q^-\rangle$ in Eqs. (2) and (3) with $\sum \Pi_{nq}^{jm}(\theta_1,\theta_2)\langle\sigma_j^+\rangle\langle\sigma_m^+\rangle\langle\sigma_n^-\rangle\langle\sigma_q^-\rangle$, and finally obtain $\sum \Pi_{nq}^{jm}(\theta_1,\theta_2)|\langle\sigma\rangle|^4$ for the approximation of the correlation function within the relative accuracy of the order of N^{-2}, which is essentially a classical radiation pattern [35]. However, one can extend the semiclassical approach of an interacting TLS antenna for the consideration of a noninteracting quantum TLS antenna by accounting for commutation relations of TLS operators and correlations between initial state components (it is the backbone of the recipe for the postsemiclassical approximation).

Let us illustrate this concept with our example of two-excitations initial state giving contradirectional correlations, $c_{jm} = \delta_{j,j+1}/\sqrt{N}$ for the state (5). For the quantum antenna of noninteracting TLSs the simultaneous second-order correlation function in the far-field zone for the two-excitations state (5) reads as [29] $G^{(2)}(\theta_1,\theta_2;t) = |R(\theta_1,\theta_2,t)|^2$, with

$$R(\theta_1,\theta_2,t) = \langle \mathrm{vac}|\langle -|E(\theta_1,t)E(\theta_2,t)|\psi\rangle|\mathrm{vac}\rangle \propto \times \sum_{j=1}^{N-1}\sum_{l=1,2}\exp\{i\phi_j(\theta_l) + i\phi_{j+1}(\theta_{3-l})\} \times \langle -|\sigma_j^-(t)\sigma_{j+1}^-(t)|\psi\rangle, \quad (16)$$

where $E(\theta_1,t)$ is the field operator, $\phi_j(\theta_l) = k\Delta\cos\theta_l$, and $\langle -|$ is the bra vector denoting the ground state of all TLSs. We aim to estimate Eq. (16) semiclassically. Our recipe for this case would be to consider the antenna with interacting TLSs semiclassically for different uncorrelated initial states with a pair of neighbor TLSs in the excited state and others in the ground state, such as, e.g., $|+\rangle_1|+\rangle_2\prod_{j=3}^{N}|-\rangle_j$. Then, we would sum the results for all the initial states with phase factors given by Eq. (16), replacing $\langle -|\sigma_j^-(t)\sigma_{j+1}^-(t)|\psi\rangle$ with $\langle\sigma_j^-(t)\rangle\langle\sigma_{j+1}^-(t)\rangle$. Note that the radiation in the semiclassical approach is assumed to be initiated by a random polarization noise source. Such an approach can lead to spatial patterns of the semiclassical correlation functions which are quite close to the quantum ones even for a small number of TLSs in the antenna. This holds under the condition of a specifically correlated noise for different initial states (different states with $c_{jm} \neq 0$ in the superposition state (5) with the aim to reproduce the phase relationships between the parts of the initial superposition state. The details of the semiclassical approach are described in the Appendix.

Figure 7 shows an example of a quantum pattern of $G^{(2)}(\theta_1,\theta_2)$ for $N = 3$ and the initial state $|\psi\rangle \propto |+\rangle_1|+\rangle_2|-\rangle_3 + |-\rangle_1|+\rangle_2|+\rangle_3$ (one can easily show that $G^{(2)}(\theta_1,\theta_2) \propto 2 + 2\cos\{k\Delta(\cos\theta_1 - \cos\theta_2)\}$). Figure 8 shows examples of postsemiclassical patterns of

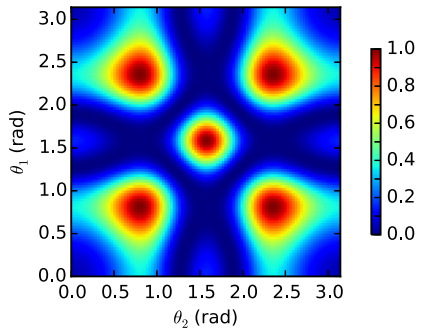

FIG. 7. The normalized (by its maximal possible value) quantum correlation function $G^{(2)}(\theta_1,\theta_2)$ for the initial state with $N = 3$ giving contradirectional twin-photon correlations. The dipole-dipole distance is $k\Delta = 4.5$.

$G^{(2)}(\theta_1,\theta_2)$ obtained with the same initial state $|\psi\rangle$ at a specific time (see Appendix). Patterns are averaged over 100 realizations with correlated (a) and uncorrelated (b) noise patterns. As shown in Figs. 7 and 8(a), for the "mirrored" realization of polarization noise for different initial states, $G^{(2)}(\theta_1,\theta_2)$ patterns for quantum and postsemiclassical cases are identical. The noise is mirrored when the jth TLS in the antenna array for the first initial state and the $N-j$th TLS of the array for the second initial state sense the same noise; see also Fig. 9(b) in the Appendix. As shown in Fig. 8(b), uncorrelated noise sources lead to a semiclassical $G^{(2)}(\theta_1,\theta_2)$ pattern with a conserved position of the maxima compared to the full quantum case, but with distortions inducing a symmetry breaking.

So, we demonstrate that it is indeed possible to use semiclassical antenna models for designing the higher-order correlation functions of the emitted field. The semiclassical approach can potentially serve as a handy

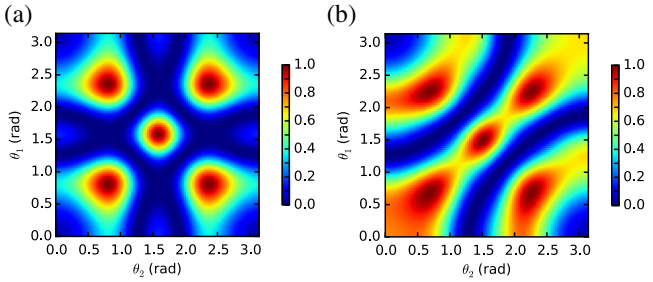

FIG. 8. The normalized (by its maximal possible value) semiclassical correlations function $G^{(2)}(\theta_1,\theta_2)$ for the initial state with $N = 3$ giving contradirectional twin-photon correlations. The semiclassical solution is given by Eq. (16) and Eqs. (17) in the Appendix. Panel (a) displays the postsemiclassical solution for correlated, "mirrored" noise sources. Panel (b) displays the semiclassical solution for uncorrelated noise sources. The patterns are taken at a specific time and are averaged over 100 realizations (see Appendix). Other parameters are as for Fig. 7.

modeling tool, because the number of equations to solve scales linearly with the number of the TLSs.

VIII. CONCLUSIONS

We show that it is possible to shape the second- and higher-order correlation functions of the field emitted by a quantum antenna in the far-field zone by designing its initial state. We propose an optimization method using constrained linear and nonlinear programming. We demonstrate the feasibility of the method for designing states with two initial excitations. We find states leading to highly co- or contradirectional emission of photon pairs for the same antenna, or even producing the effect of nonradiating sources by suppressing the field in the far-field zone. We also show that a quantum antenna can produce multiphoton momentum-entangled states. Despite the general quantum character of the state expected to produce desired spatial patterns of the correlation functions, we also demonstrate that one can still use an appropriately modified semiclassical approach for this purpose. We believe that our method for producing patterned higher-order correlation functions of the emitted field can be of importance for imaging and high-precision sensing, as well as for designing an emitter-field interface for quantum information processing [14,15,21,37,38]. In practice, the considered quantum antennas can be realized in a number of different ways, such as chains of semiconductor quantum dots [7–9], cold atoms in optical lattices [39,40], as well as nanoscale Josephson junctions [41].

ACKNOWLEDGMENTS

A. M., D. M., I. K., G. B., and D. B. acknowledge support from the EU project Horizon-2020 SUPERTWIN id.686731, the National Academy of Sciences of Belarus program "Convergence," and the BRRFI Project No. F17Y-004. G. Ya. S. acknowledges support from the Project No. FP7-612285 CANTOR. G. B. and D. B. acknowledge Philippe Renevey for advice in coding.

APPENDIX: SEMICLASSICAL MAXWELL-BLOCH MODEL OF INTERACTING DIPOLES

We consider a regular linear chain of atoms modeled with a system of N two-level atoms at equidistant positions in space given by the position vectors $\vec{R}_j$ (see Fig. 1 of the main text). A semiclassical treatment of such a system, making use of the slowly varying envelope approximation and the rotating wave approximation approximations, leads to a set of so-called Maxwell-Bloch equations (see, e.g., Chaps. 1 and 6 in Ref. [35]). Introducing relaxation processes and spontaneous fluctuations of the electric polarization in the medium under the form of a Langevin force term at each dipole (noise sources), we obtain the set of differential equations below:

$$\frac{d}{d\tau}\mathcal{R}^{(j)}(\tau) = -i\frac{\vec{d}_j}{\hbar}\vec{E}_j(\tau)\mathcal{Z}^{(j)}(\tau) - \frac{\mathcal{R}^{(j)}(\tau)}{\tau_2} + \mathcal{L}^{(j)}(\tau),$$
$$\frac{d}{d\tau}\mathcal{Z}^{(j)}(\tau) = \frac{1}{2}\left(i\frac{\vec{d}_j}{\hbar}\vec{E}_j(\tau)\mathcal{R}^{(j)*}(\tau) + \text{c.c.}\right) - \frac{1+\mathcal{Z}^{(j)}(\tau)}{\tau_1}, \tag{A1}$$

where $\mathcal{Z}^{(j)}(\tau)$ and $\mathcal{R}^{(j)}(\tau)$ correspond to the population difference and polarization (or coherence) of the jth atom, respectively, and also to the diagonal and off-diagonal elements of the single-atom density matrix, respectively. $\mathcal{L}^{(j)}(\tau)$ is the Langevin force term (noise source) applied to the jth atom. τ_1 and τ_2 are the relaxation times for inversion and macroscopic polarization, respectively. $\vec{d}_j$ is the transition dipole moment of the jth atom, and $\vec{E}_j(\tau)$ is the electric field acting on the jth atom at the position $\vec{R}_j$. This field is a superposition of the microscopic fields $\vec{E}_{lj}(\tau)$ produced at the point $\vec{R}_j$ by all other atoms labeled with index l, reading

$$\vec{E}_j(\tau) = \sum_{l\neq j}\vec{E}_{lj}(\tau), \tag{A2}$$

where the amplitudes $\vec{E}_{lj}(\tau)$ are given by

$$\vec{E}_{lj}(\tau) = \left[\frac{3}{\Delta_{lj}^3} - \frac{3ik}{\Delta_{lj}^2} - \frac{k^2}{\Delta_{lj}}\right] \times (\vec{d}_j\vec{n}_{lj})\vec{n}_{lj}\mathcal{R}^{(l)}(\tau)e^{ik\Delta_{lj}} - \left[\frac{1}{\Delta_{lj}^3} - \frac{ik}{\Delta_{lj}^2} - \frac{k^2}{\Delta_{lj}}\right]\vec{d}_j\mathcal{R}^{(l)}(\tau)e^{ik\Delta_{lj}}. \tag{A3}$$

Note that here we neglect the retardation in the amplitudes $\mathcal{R}^{(j)}(\tau)$, since we assume that the time for light to propagate through the system, L/c, is shorter than the characteristic superradiance (SR) time T_R, which defines the instability increment and the growth rate of the collective superradiant pulse [34]. To favor SR emission from our system of interacting TLS, the relaxation time τ_1 and decoherence time τ_2 used in the modeling are much longer than T_R. As one more simplification, we consider dipole matrix elements $\vec{d}_l$ of individual TLS pointing up normally with respect to the chain axis (as it is assumed in the main text), so the first term on the right-hand side of expression (A3) vanishes.

The component of the classical Poynting vector along the antenna axis takes the form

$$S(\mathbf{r},\tau) \propto \sum_{l,m}\mathcal{R}^{(l)*}(\tau)\mathcal{R}^{(m)}(\tau)e^{ik\Delta_{lm}\cos(\theta)}, \tag{A4}$$

where θ is the angle between the linear array antenna and the direction of observation, and τ is the time at the observer position.

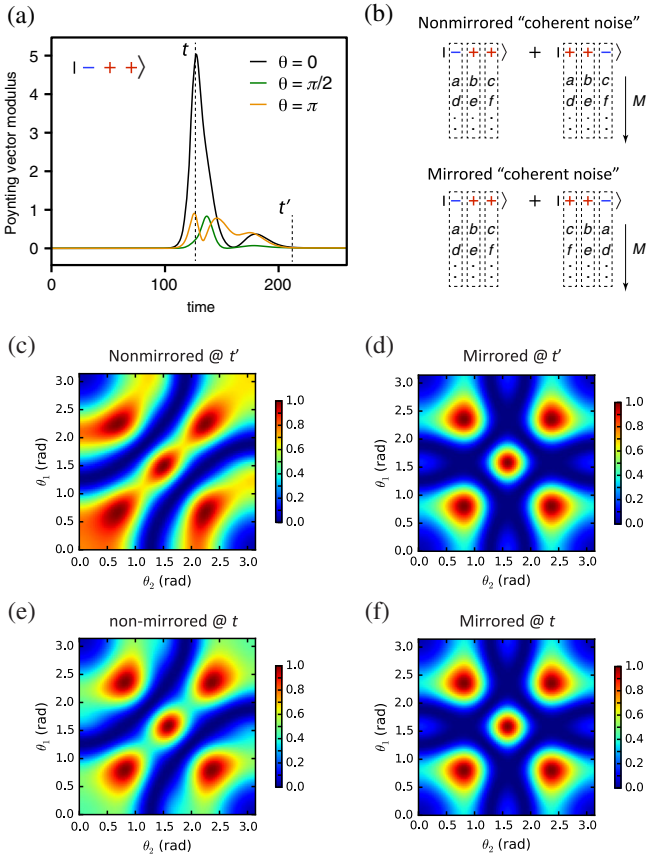

FIG. 9. (a) Example of a superradiant pulse emitted by a linear chain of three dipoles with the initial conditions $\mathcal{Z}^{(1)}(0) = -1$, $\mathcal{Z}^{(2)}(0) = \mathcal{Z}^{(3)}(0) = 1$, and $\mathcal{R}^{(1)}(0) = \mathcal{R}^{(2)}(0) = \mathcal{R}^{(3)}(0) = 0$ for $k\Delta = 4.5$. Three observation angles $\theta = \{0, \pi/2, \pi\}$ are considered. (b) Schematics of the noise source configurations for the nonmirrored and mirrored cases. Letters a, b, c, etc., correspond to different noise patterns. (c)–(f) Different normalized (by its maximal possible value) $G^{(2)}(\theta_1, \theta_2)$ patterns for both noise configurations and at times t and t' in panel (a), each for 100 realizations.

An example of a superradiant pulse emitted by a linear chain of three dipoles with the initial conditions $\mathcal{Z}^{(1)}(0) = -1$, $\mathcal{Z}^{(2)}(0) = \mathcal{Z}^{(3)}(0) = 1$ and $\mathcal{R}^{(1)}(0) = \mathcal{R}^{(2)}(0) = \mathcal{R}^{(3)}(0) = 0$ is shown in Fig. 9 for $\kappa\Delta = 4.5$, and $\mathcal{L}^{(k)}(\tau)$ being a zero-mean Gaussian noise. Three observation angles $\theta = \{0, \pi/2, \pi\}$ are considered.

It can be shown that the second-order correlation function $G^{(2)}(\theta_1, \theta_2)$ for the semiclassical case given by Eq. (16) in the main text takes here the form $G^{(2)}(\theta_1, \theta_2) = |\mathcal{A}(\theta_1, \theta_2)|^2$, where the amplitude $\mathcal{A}(\theta_1, \theta_2)$ is given as

$$\mathcal{A}(\theta_1, \theta_2) = [\mathcal{R}^{(1)}\mathcal{R}^{(2)}]_{++-}(e^{ik\Delta\cos(\theta_1)} + e^{ik\Delta\cos(\theta_2)}) + [\mathcal{R}^{(2)}\mathcal{R}^{(3)}]_{-++} \times (e^{ik\Delta[2\cos(\theta_1)+\cos(\theta_2)]} + e^{ik\Delta[\cos(\theta_1)+2\cos(\theta_2)]}),$$

where $[\mathcal{R}^{(j)}]_{++-}$ and $[\mathcal{R}^{(j)}]_{-++}$ stand for the values of the electric polarization of the jth atom for the initial states $|+\rangle_1|+\rangle_2|-\rangle_3$ and $|-\rangle_1|+\rangle_2|+\rangle_3$, respectively. Two different configurations of the noise source terms $\mathcal{L}^{(j)}(\tau)$ are considered with the so-called nonmirrored and mirrored coherent noise, as shown in Fig. 9(b).

Examples of normalized $G^{(2)}(\theta_1, \theta_2)$ functions calculated at two different times t and t' for both noise configurations are displayed in panels (c)–(f) for an averaging over 100 realizations. It can be shown that for the mirrored noise case, the pattern is time independent and is identical to the pure quantum case shown in Fig. (6) in the main text. For the nonmirrored case, the patterns are time dependent but their variation over time is small and the position of the maxima is conserved compared to the pure quantum case.

[1] C. A. Balanis, *Antenna Theory—Analysis and Design*, 3rd ed. (John Wiley and Sons, Inc., Hoboken, NJ, 2005).

[2] P. Biagioni, Y.-S. Huang, and B. Hecht, Nanoantennas for visible and infrared radiation, Rep. Prog. Phys. **75**, 024402 (2012).

[3] L. Novotny and N. van Hulst, Antennas for light, Nat. Photonics **5**, 83 (2011).

[4] A. Alu and N. Engheta, Input Impedance, Nanocircuit Loading, and Radiation Tuning of Optical Nanoantennas, Phys. Rev. Lett. **101**, 043901 (2008).

[5] J.-J. Greffet, M. Laroche, and F. Marquier, Impedance of a Nanoantenna and a Single Quantum Emitter, Phys. Rev. Lett. **105**, 117701 (2010).

[6] G. Y. Slepyan and A. Boag, Quantum Nonreciprocity of Nanoscale Antenna Arrays in Timed Dicke States, Phys. Rev. Lett. **111**, 023602 (2013).

[7] S. Mokhlespour, J. E. M. Haverkort, G. Slepyan, S. Maksimenko, and A. Hoffmann, Collective spontaneous emission in coupled quantum dots: Physical mechanism of quantum nanoantenna, Phys. Rev. B **86**, 245322 (2012).

[8] G. Y. Slepyan, Y. D. Yerchak, A. Hoffmann, and F. G. Bass, Strong electron-photon coupling in a one-dimensional quantum dot chain: Rabi waves and Rabi wave packets, Phys. Rev. B **81**, 085115 (2010).

[9] G. Ya. Slepyan, Y. D. Yerchak, S. A. Maksimenko, A. Hoffmann, and F. G. Bass, Mixed states in Rabi waves and quantum nanoantennas, Phys. Rev. B **85**, 245134 (2012).

[10] G. Ya. Slepyan, Heisenberg uncertainty principle and light squeezing in quantum nanoantennas and electric circuits, J. Nanophoton. **10**, 046005 (2016).

[11] N. Sangouard, Ch. Simon, H. de Riedmatten, and N. Gisin, Quantum repeaters based on atomic ensembles and linear optics, Rev. Mod. Phys. **83**, 33 (2011).

[12] J.-W. Pan, Z.-B. Chen, C.-Y. Lu, H. Weinfurter, A. Zeilinger, and M. Zukowski, Multi-photon entanglement and interferometry, Rev. Mod. Phys. **84**, 777 (2012).

[13] R. Wiegner, J. von Zanthier, and G. S. Agarwal, Quantum-interference-initiated superradiant and subradiant emission from entangled atoms, Phys. Rev. A **84**, 023805 (2011).

[14] A. N. Boto, P. Kok, D. S. Abrams, S. L. Braunstein, C. P. Williams, and J. P. Dowling, Quantum Interferometric

Optical Lithography: Exploiting Entanglement to Beat the Diffraction Limit, Phys. Rev. Lett. **85**, 2733 (2000).
[15] L. A. Rozema, J. D. Bateman, D. H. Mahler, R. Okamoto, A. Feizpour, A. Hayat, and A. M. Steinberg, Scalable Spatial Superresolution Using Entangled Photons, Phys. Rev. Lett. **112**, 223602 (2014).
[16] D. Bhatti, J. von Zanthier, and G. S. Agarwal, Superbunching and nonclassicality as new hallmarks of superradiance, Sci. Rep. **5**, 17335 (2015).
[17] M. O. Scully, E. S. Fry, C. H. Raymond Ooi, and K. Wódkiewicz, Directed Spontaneous Emission from an Extended Ensemble of N Atoms: Timing Is Everything, Phys. Rev. Lett. **96**, 010501 (2006).
[18] M. Cassano, M. D'Angelo, A. Garuccio, T. Peng, Y. Shih, and V. Tamma, Spatial interference between pairs of disjoint optical paths with a single chaotic source, Opt. Express **25**, 6589 (2017).
[19] S. Oppel, T. Buttner, P. Kok, and J. von Zanthier, Superresolving Multiphoton Interferences with Independent Light Sources, Phys. Rev. Lett. **109**, 233603 (2012).
[20] A. Classen, F. Waldmann, S. Giebel, R. Schneider, D. Bhatti, Th. Mehringer, and J. von Zanthier, Superresolving Imaging of Arbitrary One-Dimensional Arrays of Thermal Light Sources Using Multiphoton Interference, Phys. Rev. Lett. **117**, 253601 (2016).
[21] http://www.supertwin.eu/.
[22] A. J. Devaney and E. Wolf, Radiating and nonradiating classical current distributions and the fields they generate, Phys. Rev. D **8**, 1044 (1973).
[23] Z. Hradil, D. Mogilevtsev, and J. Řeháček, Biased Tomography Schemes: An Objective Approach, Phys. Rev. Lett. **96**, 230401 (2006); D. Mogilevtsev, J. Řeháček, and Z. Hradil, Objective approach to biased tomography schemes, Phys. Rev. A **75**, 012112 (2007).
[24] M. D. Lukin and P. R. Hemmer, Quantum Entanglement via Optical Control of Atom-Atom Interactions, Phys. Rev. Lett. **84**, 2818 (2000).
[25] M. Saffman and T. G. Walker, Quantum information with Rydberg atoms, Rev. Mod. Phys. **82**, 2313 (2010).
[26] R. Blatt and D. Wineland, Entangled states of trapped atomic ions, Nature (London) **453**, 1008 (2008).
[27] A. I. Lvovsky, B. C. Sanders, and W. Tittel, Optical quantum memory, Nat. Photonics **3**, 706 (2009).
[28] F. Bussieres, N. Sangouard, M. Afzelius, H. de Riedmatten, Ch. Simon, and W. Tittel, Prospective applications of optical quantum memories, J. Mod. Opt. **60**, 1519 (2013).
[29] M. O. Scully and M. Zubairy, *Quantum Optics* (Cambridge University Press, Cambridge, 2001).
[30] S. V. Gaponenko, *Introduction to Nanophotonics* (Cambridge University Press, Cambridge, 2010).
[31] W. Cai and V. M. Shalaev, *Optical Metamaterials* (Springer, New York, 2010).
[32] G. Slepyan, A. Boag, V. Mordachev, E. Sinkevich, S. Maksimenko, P. Kuzhir, G. Miano, M. E. Portnoi, and A. Maffucci, Anomalous electromagnetic coupling via entanglement at the nanoscale, New J. Phys. **19**, 023014 (2017).
[33] R. Tanas and Z. Ficek, Entangling two atoms via spontaneous emission, J. Opt. B **6**, S90 (2004).
[34] D. L. Boiko and P. P. Vasilev, Superradiance dynamics in semiconductor laser diode structures, Opt. Express **20**, 9501 (2012).
[35] M. G. Benedict, A. M. Ermolaev, V. A. Malyshev, I. V. Sokolov, and E. D. Trifonov, Super-Radiance: Multiatomic Coherent Emission, *Optics and Optoelectronics* (IOP Publishing Ltd., Bristol, U.K., 1996).
[36] Z. Ficek, R. Tanas, and S. Kielich, Quantum beats and superradiant effects in the spontaneous emission from two nonidentical atoms, Physica (Amsterdam) **146A**, 452 (1987).
[37] B. le Feber, N. Rotenberg, and L. Kuipers, Nanophotonic control of circular dipole emission, Nat. Commun. **6**, 6695 (2015).
[38] S. Checcucci, P. Lombardi, S. Rizvi, F. Sgrignuoli, N. Gruhler, F. B. C. Dieleman, F. S. Cataliotti, W. H. P. Pernice, M. Agio, and C. Toninelli, Beaming light from a quantum emitter with a planar optical antenna, Light Sci. Appl. **6**, e16245 (2017).
[39] M. Ben Dahan, E. Peik, J. Reichel, Y. Castin, and Ch. Salomon, Bloch Oscillations of Atoms in an Optical Potential, Phys. Rev. Lett. **76**, 4508 (1996).
[40] E. Haller, R. Hart, M. J. Mark, J. G. Danzl, L. Reichsollner, and H.-Ch. Nagerl, Inducing Transport in a Dissipation-Free Lattice with Super Bloch Oscillations, Phys. Rev. Lett. **104**, 200403 (2010).
[41] H. Vora, R. L. Kautz, S. W. Nam, and J. Aumentado, Modeling Bloch oscillations in nanoscale Josephson junctions, Phys. Rev. B **96**, 054505 (2017).

Correction: The images in Figs. 7–9 did not convert properly and have been successfully reprocessed.